Biomedical Optics EXPRESS

Sensitivity of MRI-guided near-infrared spectroscopy clinical breast exam data and its impact on diagnostic performance

Michael A. Mastanduno,[1,4] Junqing Xu,[2,4] Fadi El-Ghussein,[1] Shudong Jiang,[1] Hong Yin,[2,*] Yan Zhao,[1] Kelly E. Michaelson,[1] Ke Wang,[2] Fang Ren,[2] Brian W. Pogue,[1] and Keith D. Paulsen[1,3,*]

[1]*Thayer School of Engineering, Dartmouth College, Hanover NH 03755 USA*
[2]*Department of Radiology, Xijing Hospital, Fourth Military Medical University, Xian, 710032 China*
[3]*Department of Diagnostic Radiology, Dartmouth College, Hanover, NH03755 USA*
[4]*Authors contributed equally to the work*
[*]*yinhong@fmmu.edu.cn*
[*]*keith.d.paulsen@dartmouth.edu*

Abstract: In this study, data from breast MRI-guided near infrared spectroscopy (NIRS) exams delivered to 44 patients scheduled for surgical resection (ending in 16 benign and 28 malignant diagnoses) were analyzed using a spatial sensitivity metric to quantify the adequacy of the optical measurements for interrogating the tumor region of interest, as derived from the concurrent MRI scan. Along with positional sensitivity, the incorporation of spectral priors and the selection of an appropriate regularization parameter in the image reconstruction were considered, and found to influence the diagnostic accuracy of the recovered images. Once optimized, the MRI/NIRS data was able to differentiate the malignant from benign lesions through both total hemoglobin ($p = 0.0037$) and tissue optical index ($p = 0.00019$), but required the relative spatial sensitivity of the optical measurement data to each lesion to be above 1%. Spectral constraints implemented during the reconstruction were required to obtain statistically significant diagnostic information from images of H_2O, lipids, and Tissue Optical Index (TOI). These results confirm the need for optical systems that have homogenous spatial coverage of the breast while still being able to accommodate the normal range of breast sizes.

OCIS codes: (170.0110) Imaging systems; (170.6960) Tomography; (100.6890) Three-dimensional image processing.

References and links

1. P. Skaane, S. Hofvind, and A. Skjennald, "Randomized trial of screen-film versus full-field digital mammography with soft-copy reading in population-based screening program: follow-up and final results of Oslo II study," Radiology **244**(3), 708–717 (2007).
2. E. D. Pisano, C. Gatsonis, E. Hendrick, M. Yaffe, J. K. Baum, S. Acharyya, E. F. Conant, L. L. Fajardo, L. Bassett, C. D'Orsi, R. Jong, and M. Rebner; Digital Mammographic Imaging Screening Trial (DMIST) Investigators Group, "Diagnostic performance of digital versus film mammography for breast-cancer screening," N. Engl. J. Med. **353**(17), 1773–1783 (2005).
3. M. D. Schnall, "Application of magnetic resonance imaging to early detection of breast cancer," Breast Cancer Res. **3**(1), 17–21 (2001).
4. E. Warner, D. B. Plewes, R. S. Shumak, G. C. Catzavelos, L. S. Di Prospero, M. J. Yaffe, V. Goel, E. Ramsay, P. L. Chart, D. E. Cole, G. A. Taylor, M. Cutrara, T. H. Samuels, J. P. Murphy, J. M. Murphy, and S. A. Narod, "Comparison of breast magnetic resonance imaging, mammography, and ultrasound for surveillance of women at high risk for hereditary breast cancer," J. Clin. Oncol. **19**(15), 3524–3531 (2001).
5. M. J. Stoutjesdijk, C. Boetes, G. J. Jager, L. Beex, P. Bult, J. H. Hendriks, R. J. Laheij, L. Massuger, L. E. van Die, T. Wobbes, and J. O. Barentsz, "Magnetic resonance imaging and mammography in women with a hereditary risk of breast cancer," J. Natl. Cancer Inst. **93**(14), 1095–1102 (2001).
6. L. Liberman, E. A. Morris, C. M. Kim, J. B. Kaplan, A. F. Abramson, J. H. Menell, K. J. Van Zee, and D. D. Dershaw, "MR imaging findings in the contralateral breast of women with recently diagnosed breast cancer," AJR Am. J. Roentgenol. **180**(2), 333–341 (2003).

#214026 - $15.00 USD Received 16 Jun 2014; revised 8 Aug 2014; accepted 8 Aug 2014; published 22 Aug 2014

7. E. A. Morris, L. Liberman, D. J. Ballon, M. Robson, A. F. Abramson, A. Heerdt, and D. D. Dershaw, "MRI of occult breast carcinoma in a high-risk population," AJR Am. J. Roentgenol. **181**(3), 619–626 (2003).
8. D. A. Bluemke, C. A. Gatsonis, M. H. Chen, G. A. DeAngelis, N. DeBruhl, S. Harms, S. H. Heywang-Köbrunner, N. Hylton, C. K. Kuhl, C. Lehman, E. D. Pisano, P. Causer, S. J. Schnitt, S. F. Smazal, C. B. Stelling, P. T. Weatherall, and M. D. Schnall, "Magnetic resonance imaging of the breast prior to biopsy," JAMA **292**(22), 2735–2742 (2004).
9. C. D. Lehman, C. Gatsonis, C. K. Kuhl, R. E. Hendrick, E. D. Pisano, L. Hanna, S. Peacock, S. F. Smazal, D. D. Maki, T. B. Julian, E. R. DePeri, D. A. Bluemke, and M. D. Schnall; ACRIN Trial 6667 Investigators Group, "MRI evaluation of the contralateral breast in women with recently diagnosed breast cancer," N. Engl. J. Med. **356**(13), 1295–1303 (2007).
10. S. J. Lord, W. Lei, P. Craft, J. N. Cawson, I. Morris, S. Walleser, A. Griffiths, S. Parker, and N. Houssami, "A systematic review of the effectiveness of magnetic resonance imaging (MRI) as an addition to mammography and ultrasound in screening young women at high risk of breast cancer," Eur. J. Cancer **43**(13), 1905–1917 (2007).
11. E. Warner, H. Messersmith, P. Causer, A. Eisen, R. Shumak, and D. Plewes, "Systematic review: using magnetic resonance imaging to screen women at high risk for breast cancer," Ann. Intern. Med. **148**(9), 671–679 (2008).
12. K. K. Lindfors, J. M. Boone, T. R. Nelson, K. Yang, A. L. C. Kwan, and D. F. Miller, "Dedicated breast CT: initial clinical experience," Radiology **246**(3), 725–733 (2008).
13. J. M. Park, E. A. Franken, Jr., M. Garg, L. L. Fajardo, and L. T. Niklason, "Breast tomosynthesis: present considerations and future applications," Radiographics **27**(Suppl 1), S231–S240 (2007).
14. S. P. Poplack, T. D. Tosteson, C. A. Kogel, and H. M. Nagy, "Digital breast tomosynthesis: initial experience in 98 women with abnormal digital screening mammography," AJR Am. J. Roentgenol. **189**(3), 616–623 (2007).
15. S. G. Orel and M. D. Schnall, "MR imaging of the breast for the detection, diagnosis, and staging of breast cancer," Radiology **220**(1), 13–30 (2001).
16. L. Bartella, C. S. Smith, D. D. Dershaw, and L. Liberman, "Imaging breast cancer," Radiol. Clin. North Am. **45**(1), 45–67 (2007).
17. V. Ntziachristos, A. G. Yodh, M. Schnall, and B. Chance, "Concurrent MRI and diffuse optical tomography of breast after indocyanine green enhancement," Proc. Natl. Acad. Sci. U.S.A. **97**(6), 2767–2772 (2000).
18. C. M. Carpenter, B. W. Pogue, S. J. Jiang, H. Dehghani, X. Wang, K. D. Paulsen, W. A. Wells, J. Forero, C. Kogel, J. B. Weaver, S. P. Poplack, and P. A. Kaufman, "Image-guided optical spectroscopy provides molecular-specific information in vivo: MRI-guided spectroscopy of breast cancer hemoglobin, water, and scatterer size," Opt. Lett. **32**(8), 933–935 (2007).
19. G. Gulsen, O. Birgul, M. B. Unlu, R. Shafiiha, and O. Nalcioglu, "Combined Diffuse Optical Tomography (DOT) and MRI System for Cancer Imaging in Small Animals," Technol. Cancer Res. Treat. **5**(4), 351–363 (2006).
20. S. C. Davis, B. W. Pogue, R. Springett, C. Leussler, P. Mazurkewitz, S. B. Tuttle, S. L. Gibbs-Strauss, S. S. Jiang, H. Dehghani, and K. D. Paulsen, "Magnetic Resonance-Coupled Fluorescence Tomography Scanner for Molecular Imaging of Tissue," Rev. Sci. Instrum. **79**(6), 064302 (2008).
21. B. J. Tromberg, B. W. Pogue, K. D. Paulsen, A. G. Yodh, D. A. Boas, and A. E. Cerussi, "Assessing the future of diffuse optical imaging technologies for breast cancer management," Med. Phys. **35**(6), 2443–2451 (2008).
22. C. M. Carpenter, R. Rakow-Penner, S. Jiang, B. L. Daniel, B. W. Pogue, G. H. Glover, and K. D. Paulsen, "Inspired gas-induced vascular change in tumors with magnetic-resonance-guided near-infrared imaging: human breast pilot study," J. Biomed. Opt. **15**(3), 036026 (2010).
23. B. Brooksby, S. Jiang, H. Dehghani, B. W. Pogue, K. D. Paulsen, J. Weaver, C. Kogel, and S. P. Poplack, "Combining near-infrared tomography and magnetic resonance imaging to study in vivo breast tissue: implementation of a Laplacian-type regularization to incorporate magnetic resonance structure," J. Biomed. Opt. **10**(5), 051504 (2005).
24. C. M. Carpenter, S. Srinivasan, B. W. Pogue, and K. D. Paulsen, "Methodology development for three-dimensional MR-guided near infrared spectroscopy of breast tumors," Opt. Express **16**(22), 17903–17914 (2008).
25. B. Brooksby, S. D. Jiang, H. Dehghani, B. W. Pogue, K. D. Paulsen, C. Kogel, M. Doyley, J. B. Weaver, and S. P. Poplack, "Magnetic resonance-guided near-infrared tomography of the breast," Rev. Sci. Instrum. **75**(12), 5262–5270 (2004).
26. M. A. Mastanduno, F. El-Ghussein, S. Jiang, R. Diflorio-Alexander, X. Junqing, Y. Hong, B. W. Pogue, and K. D. Paulsen, "Adaptable Near-Infrared Spectroscopy Fiber Array for Improved Coupling to Different Breast Sizes During Clinical MRI," Acad. Radiol. **21**(2), 141–150 (2014).
27. H. Dehghani, M. E. Eames, P. K. Yalavarthy, S. C. Davis, S. Srinivasan, C. M. Carpenter, B. W. Pogue, and K. D. Paulsen, "Near infrared optical tomography using NIRFAST: Algorithm for numerical model and image reconstruction," Commun. Numer. Methods Eng. **25**(6), 711–732 (2009).
28. S. R. Arridge and M. Schweiger, "Photon-measurement density functions. Part 2: Finite-element-method calculations," Appl. Opt. **34**(34), 8026–8037 (1995).
29. H. J. van Staveren, C. J. M. Moes, J. van Marie, S. A. Prahl, and M. J. C. van Gemert, "Light Scattering in Intralipid-10% in the wavelength range of 400-1100 nm," Appl. Opt. **30**(31), 4507–4514 (1991).
30. J. R. Mourant, T. Fuselier, J. Boyer, T. M. Johnson, and I. J. Bigio, "Predictions and measurements of scattering and absorption over broad wavelength ranges in tissue phantoms," Appl. Opt. **36**(4), 949–957 (1997).
31. S. Srinivasan, B. W. Pogue, S. Jiang, H. Dehghani, and K. D. Paulsen, "Spectrally constrained chromophore and scattering near-infrared tomography provides quantitative and robust reconstruction," Appl. Opt. **44**(10), 1858–1869 (2005).

#214026 - $15.00 USD Received 16 Jun 2014; revised 8 Aug 2014; accepted 8 Aug 2014; published 22 Aug 2014

32. S. Srinivasan, B. W. Pogue, B. Brooksby, S. Jiang, H. Dehghani, C. Kogel, W. A. Wells, S. P. Poplack, and K. D. Paulsen, "Near-infrared characterization of breast tumors in vivo using spectrally-constrained reconstruction," Technol. Cancer Res. Treat. **4**(5), 513–526 (2005).
33. S. C. Davis, H. Dehghani, P. K. Yalavarthy, B. W. Pogue, and K. D. Paulsen, "Comparing two regularization techniques for diffuse optical tomography," in (2007), Vol. 6434, p. 64340X–64340X–12.
34. M. A. Mastanduno, S. Jiang, R. DiFlorio-Alexander, B. W. Pogue, and K. D. Paulsen, "Remote positioning optical breast magnetic resonance coil for slice-selection during image-guided near-infrared spectroscopy of breast cancer," J. Biomed. Opt. **16**(6), 066001 (2011).
35. H. Dehghani, B. W. Pogue, J. Shudong, B. Brooksby, and K. D. Paulsen, "Three-dimensional optical tomography: resolution in small-object imaging," Appl. Opt. **42**(16), 3117–3128 (2003).
36. B. W. Pogue, S. C. Davis, X. Song, B. A. Brooksby, H. Dehghani, and K. D. Paulsen, "Image analysis methods for diffuse optical tomography," J. Biomed. Opt. **11**(3), 033001 (2006).
37. H. R. Ghadyani, S. Srinivasan, B. W. Pogue, and K. D. Paulsen, "Characterizing accuracy of total hemoglobin recovery using contrast-detail analysis in 3D image-guided near infrared spectroscopy with the boundary element method," Opt. Express **18**(15), 15917–15935 (2010).
38. B. Brooksby, S. Srinivasan, S. Jiang, H. Dehghani, B. W. Pogue, K. D. Paulsen, J. Weaver, C. Kogel, and S. P. Poplack, "Spectral priors improve near-infrared diffuse tomography more than spatial priors," Opt. Lett. **30**(15), 1968–1970 (2005).
39. A. Li, G. Boverman, Y. Zhang, D. Brooks, E. L. Miller, M. E. Kilmer, Q. Zhang, E. M. C. Hillman, and D. A. Boas, "Optimal linear inverse solution with multiple priors in diffuse optical tomography," Appl. Opt. **44**(10), 1948–1956 (2005).
40. M. Guven, B. Yazici, X. Intes, and B. Chance, "Diffuse optical tomography with a priori anatomical information," Phys. Med. Biol. **50**(12), 2837–2858 (2005).
41. B. A. Brooksby, H. Dehghani, B. W. Pogue, and K. D. Paulsen, "Near-infrared tomography breast image reconstruction with a priori structural information from MRI: algorithm development for reconstructing heterogeneities," IEEE J. Sel. Top. Quantum Electron. **9**, 199–209 (2003).
42. Q. Zhu, P. U. Hegde, A. Ricci, Jr., M. Kane, E. B. Cronin, Y. Ardeshirpour, C. Xu, A. Aguirre, S. H. Kurtzman, P. J. Deckers, and S. H. Tannenbaum, "Early-Stage Invasive Breast Cancers: Potential Role of Optical Tomography with US Localization in Assisting Diagnosis," Radiology **256**(2), 367–378 (2010).
43. R. Choe, S. D. Konecky, A. Corlu, K. Lee, T. Durduran, D. R. Busch, B. Czerniecki, J. Tchou, D. L. Fraker, A. DeMichele, B. Chance, E. Putt, M. D. Schnall, M. A. Rosen, and A. G. Yodh, "Differentiation of benign and malignant breast lesions by in-vivo three-dimensional diffuse optical tomography," Cancer Res. **69**(2 Supplement), 102S (2009).
44. C. M. Carpenter, B. W. Pogue, S. Jiang, J. Wang, B. A. Hargreaves, R. Rakow-Penner, B. L. Daniel, and K. D. Paulsen, "MR Water Quantitative Priors Improves the Accuracy of Optical Breast Imaging," IEEE Trans. Med. Imaging **30**(1), 159–168 (2011).
45. B. W. Pogue, S. C. Davis, F. Leblond, M. A. Mastanduno, H. Dehghani, and K. D. Paulsen, "Implicit and explicit prior information in near-infrared spectral imaging: accuracy, quantification and diagnostic value," Philos Trans. Math Phys. Eng. Sci. **369**(1955), 4531–4557 (2011).
46. S. C. Davis, K. S. Samkoe, J. A. O'Hara, S. L. Gibbs-Strauss, H. L. Payne, P. J. Hoopes, K. D. Paulsen, and B. W. Pogue, "MRI-coupled Fluorescence Tomography Quantifies EGFR Activity in Brain Tumors," Acad. Radiol. **17**(3), 271–276 (2010).
47. B. Brooksby, B. W. Pogue, S. Jiang, H. Dehghani, S. Srinivasan, C. Kogel, T. D. Tosteson, J. B. Weaver, S. P. Poplack, and K. D. Paulsen, "Imaging Breast Adipose and Fibroglandular Tissue Molecular Signatures by using Hybrid MRI-Guided Near-Infrared Spectral Tomography," Proc. Natl. Acad. Sci. U.S.A. **103**(23), 8828–8833 (2006).
48. S. Kukreti, A. E. Cerussi, W. Tanamai, D. Hsiang, B. J. Tromberg, and E. Gratton, "Characterization of Metabolic Differences between Benign and Malignant Tumors: High-Spectral-Resolution Diffuse Optical Spectroscopy," Radiology **254**(1), 277–284 (2010).

1. Introduction

Breast cancer is a complex and diverse disease that is routinely screened using x-ray mammography, which has an overall sensitivity and specificity reported to be in the mid-70s and high-90s, respectively, (e.g. in a relatively recent randomized multi-center trial [1]), although sensitivity has been found to be as low as 40% in some large trials [2]. Unfortunately, its effectiveness in women with mammographically dense breasts is reduced, especially sensitivity, which drops into the 60% range (as low as 36% in [2]). Clinically, MRI is the most sensitive exam for cancer surveillance, especially in the dense breast [3–9], and national guidelines now recommend routine breast MR screening in women with an elevated lifetime breast cancer risk of 20% or more [10,11]. Thus, even with pressures from healthcare cost containment, the emergence of x-ray tomographic systems [12–14], and the relative expense of an exam, the number of breast MR studies can be expected to grow in the future because of the exquisite soft-tissue delineation that is provided. However, breast MRI has a substantial false positive rate [15,16] due to its reliance on gadolinium (Gd) as a non-specific

#214026 - $15.00 USD Received 16 Jun 2014; revised 8 Aug 2014; accepted 8 Aug 2014; published 22 Aug 2014

contrast agent. The number of false positives caused by the technique is particularly troubling because of the clinical management burden that is created by the increase in contrast-enhancing foci that need to be evaluated. As a result, supplementing the diagnostic information derived from MR would have significant clinical impact, especially if the adjunctive data were coregistered with the MR image volume and could be seamlessly acquired during the same procedure.

Combined MRI/optical imaging is an emerging multi-modality technology [17–20] that could benefit the diagnoses of patients called back after screening for further testing or women at high-risk initially screened with MRI by adding functional information about the molecular status of the breast [21] through the optical technique which non-invasively quantifies oxy- and deoxy-hemoglobin (HbO and Hb), water and lipid content, and scattering parameters in adipose and fibroglandular tissues. To date, evidence for the potential promise of MRI/optical imaging has mostly been limited to anecdotal case studies [18,22], and the approach remains largely untested in a patient population of any size. As a result, important methodological issues specific to human imaging that are related to the non-linear sensitivity of diffuse optical methods have not been studied. For example, optical imaging is well known to lack sensitivity to 1) deeper lesions, 2) lesions distant from measurement locations, or 3) lesions that are small in size, but the quality of the data and associated images that can be acquired clinically is not as well understood because of the relatively limited testing on humans, especially when the technique is augmented with priors from another imaging modality, in this case, MRI.

Our MRI/optical imaging has been under development for several years [23–26], and was deployed to evaluate the sensitivity of the data that can be routinely acquired during a clinical breast exam. Specifically, we generated a sensitivity map before image reconstruction to minimize over-interpretation of lesions with low sensitivity to the data collected, and identified criteria for data inclusion based on breast exam data acquired from a cohort of 44 women with breast abnormalities. To the best of our knowledge, no other method exists to quantify, objectively, if and when the optical measurement data can be expected to recover accurate information about a particular lesion or region of interest in MRI/optical breast imaging. Non-linear image reconstruction includes both spatial and spectral constraints that can be incorporated at multiple stages. A regularization parameter must also be selected to maintain image stability while not over damping image contrast. These issues are investigated using the clinical data as a vehicle for determining the choices that lead to improved diagnostic outcomes with the combined MRI/optical imaging technique.

2. Methods

2.1 Instrumentation

The MRI/optical system deployed in this study consists of six intensity modulated laser diodes and three continuous-wave laser diodes with wavelengths spanning from 660nm to 850nm, and 900nm to 950nm, respectively. Sixteen sequential source positions illuminate the breast through a custom optical switch. During each individual source illumination, the remaining 15 fibers detect transmitted light with photomultiplier tubes, PMTs (Hamamatsu, 9305-03), and large active area photodiodes (Hamamatsu C10439-03). The amplitude and phase (when available) of the detected light are separated by lock-in detection. The optical imaging hardware is located in the MR console room, and 12m fiber bundles with 4mm working optical diameters are passed through a custom penetration panel to enter the MR scanner room. These fibers are coupled into a clinical breast coil for simultaneous MR and optical imaging of patients or phantoms. Clinical MRI image quality and acquisition time are not affected by the addition of the optical fiber array. More details on the imaging instrumentation can be found in previous publications [25].

#214026 - $15.00 USD Received 16 Jun 2014; revised 8 Aug 2014; accepted 8 Aug 2014; published 22 Aug 2014

2.2 Image reconstruction

Breast images are processed and reconstructed with the open source software platform, Nirfast [27]. Briefly, the difference between measured data and a diffusion-based model of light propagation through the medium is minimized to yield estimates of the optical properties of the tissue of interest. The diffusion equation has been well studied in this setting and is an acceptable approximation in tissues where scattering (μ_s') dominates absorption (μ_a), and source-detector separation is greater than one scattering distance [28]. In an unconstrained spectral reconstruction, the image formation algorithm is non-linear and solved with a Newton-type minimization method where the mismatch between the data and the model at one wavelength is minimized by changing μ_a and μ_s'. All wavelengths are reconstructed separately for the absorption and scattering coefficients which are then combined linearly to form the relevant chromophore concentrations. From these we derive Total Hemoglobin (HbT), Oxygen Saturation (StO_2), and Tissue Optical Index (TOI) through $HbT = HbO + Hb$, $StO_2 = HbO / HbT$, and $TOI = (HbT * water) / lipid$. Similarly, scattering amplitude, A, and scattering power, b, are fit in each region to an empirically derived power law approximation to Mie Theory, $\mu_s' = a\lambda^{-b}$ [29,30].

Constrained spectral reconstruction employs spectral priors by solving for chromophores directly and simultaneously based on measurements of absorption and scatter [31,32]. The approach is faster and more robust to noise, and previous work has indicated accuracy improvements occur in the recovered chromophore concentrations when the method is applied. However, the effect of reconstruction type (constrained vs. unconstrained) has not been evaluated in a large data set of patient exams, especially in the setting of also using spatial priors. In this study, each patient was reconstructed with both constrained and unconstrained spectral algorithms to assess the value of the constrained approach. The resulting images were evaluated relative to the known surgical pathology and expected physiological conditions. Two-tailed student t-tests (significance $p<0.05$) were performed on the ratio of mean tumor to mean background levels of each chromophore. Given that each data set was used for only one test, we did not correct for multiple comparisons.

2.3 Sensitivity analysis

The Jacobian matrix in the image reconstruction process contains the spatial sensitivity of each measurement at each location within the image volume and can be used to quantify the overall sensitivity field of the measured data prior to image formation. The sensitivity of the measurements to a given region identified by MRI, S_r, can be calculated using the equation, $S_r = sum\left[\log(J \cdot r)\right]$. Here, r is a logical vector that identifies points within the region of interest and J is the Jacobian. The total sensitivity of the measurements to the domain, S_t, is obtained when r is entirely true. Regions are identified by MRI during image segmentation, and the sensitivity of the region relative to the total sensitivity can be found by S_r/S_t. Relative tumor sensitivity is a quantity that could predict reconstructed image quality by providing a quantitative metric of the overlap between the measurement sensitivity and the region of interest. Figure 1 shows a visual example of the Jacobian-calculated sensitivity in relation to the tumor location.

#214026 - $15.00 USD Received 16 Jun 2014; revised 8 Aug 2014; accepted 8 Aug 2014; published 22 Aug 2014

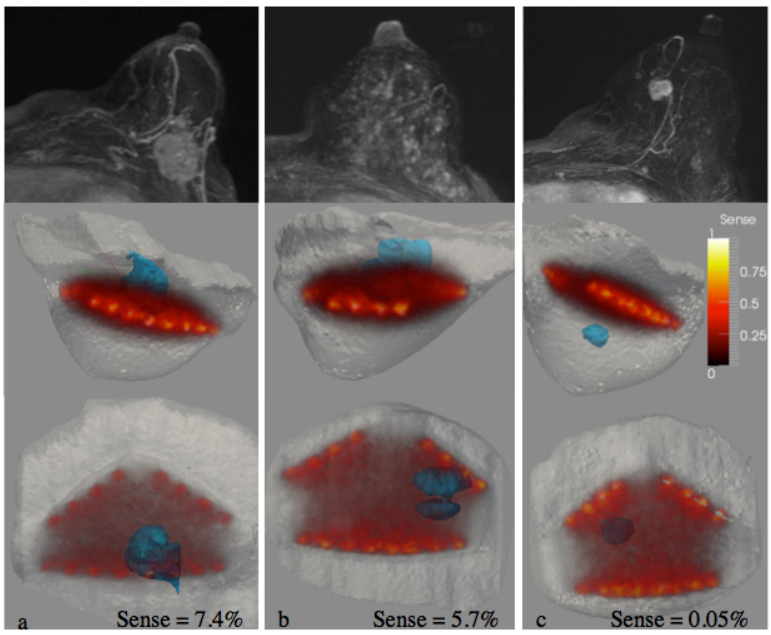

Fig. 1. The Jacobian field is plotted within the MRI image volume of 3 different breasts with lesions (found by MRI) shown in blue. The overlap between the lesion and the Jacobian yields the sensitivity of the optical measurements to the lesion. These examples illustrate two cases (a,b) with good and one case with very poor sensitivity (c).

Similarly to finding the sensitivity of each region, quantifying the sensitivity of each measurement to each region is also possible. The sensitivity of the i^{th} measurement to region r, $S_{i,r}$, can be calculated as $S_i = sum\left[\log(J(i,:)\cdot r)\right]$ where i selects the corresponding row of J, and r identifies the ROI. When this expression is applied to a given measurement, the sensitivity of the corresponding data to the lesion is found. Examples of optical measurements that possess high and low sensitivity to a lesion are illustrated in Fig. 2.

Sensitivity analysis was applied to a data set consisting of 44 combined breast MR/optical breast exams to evaluate its influence on the reconstructed results. The relative sensitivity to each lesion was calculated as described in Section 2.3.1 and subject exams were sorted by lesions being the most to the least sensitive to the optical data. Reconstructed chromophore concentrations were compared versus the gold standard of surgical pathology in patient exams with high lesion sensitivity, moderate lesion sensitivity, and low lesion sensitivity to assess the impact of the measurement sensitivity on the diagnostic performance of the optical imaging results. Here, the Jacobian calculation was used to estimate a quantitative measure of the relative sensitivity of the data to the tumor region as described in Section 2.3.1, which was applied as the basis for data inclusion.

#214026 - $15.00 USD Received 16 Jun 2014; revised 8 Aug 2014; accepted 8 Aug 2014; published 22 Aug 2014

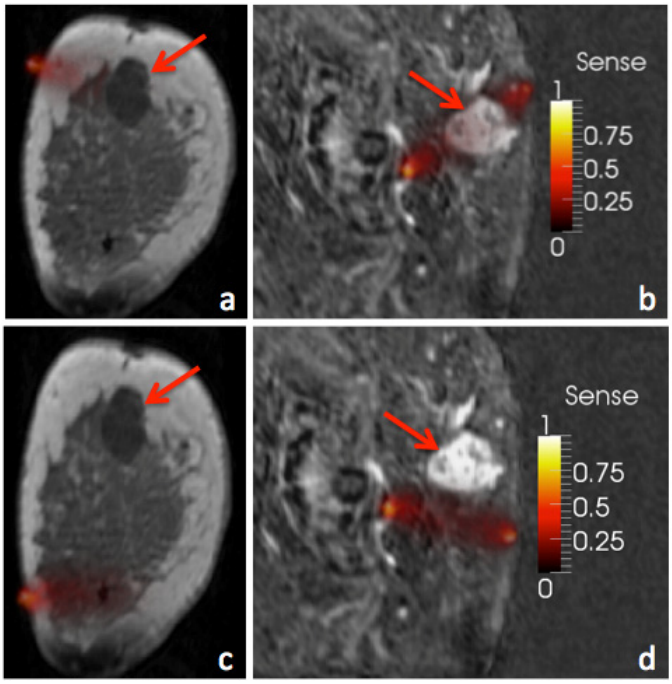

Fig. 2. Sensitivity of two measurements from two different breasts is illustrated. Measurements with high sensitivity to the tumor region (a,b) will directly impact the recovered properties of the tumor while other measurements will have much less influence (c,d).

2.4 Regularization parameters

Since the matrix to be inverted is ill-conditioned, the image formation algorithm (Eq. (1) was stabilized through a modified Tikhonov regularization routine. A single scalar parameter, λ, and identity matrix, I, make the matrix more diagonally dominant and dampens the effect of noise in the data. The model-data misfit, δ, is minimized to obtain the physiological parameters, c.

$$(J^T J + \lambda I)\Delta c = J^T \Delta \delta \tag{1}$$

Specifically, a modified Levenberg-Marquardt scheme regularized the amplitude and phase components separately, and was scaled by the maximum of the diagonal of the Hessian matrix between iterations. The reconstruction was stopped when the change between successive iterations was less than 0.2%, allowing the image reconstruction to converge slowly but robustly [33].

Three different regularization settings were evaluated in the constrained spectral reconstructions. Image results from each regularization were compared against relative tumor sensitivity, surgical pathology, and normal tissue properties to investigate the influence of regularization parameters on the clinical data.

2.5 Human Subject Imaging

Our imaging protocol for human subject examination was approved by the Committee for the Protection of Human Subjects at Dartmouth-Hitchcock Medical Center and Xijing Hospital. Written consent was obtained during which the nature of the procedure was fully explained to each volunteer. Each subject's breast was positioned into a triangular interface in the prone position on the MR exam table and the fiber optic cables were brought into contact with the breast surface. In cases of smaller breast sizes, all fibers were not in contact with the skin surface because of curvature, and data from these channels were not incorporated into the

#214026 - $15.00 USD Received 16 Jun 2014; revised 8 Aug 2014; accepted 8 Aug 2014; published 22 Aug 2014

image reconstruction. The interface involved mild compression similarly to MR biopsy plates but maintained patient comfort during the imaging procedure. Co-registration between optical and MR images was accomplished through MR fiducial markers placed in the plane of each set of fibers, and MR images were acquired with the slice-direction in the axial geometry. Optical and MR data were collected concurrently with data acquisition requiring 15 and 30 minutes, respectively. The core dynamic contrast enhanced MRI scan was a 3D, fast, low-angle shot T1 sequence acquired in the transverse plane (6.9/2.8 [repetition time msec/echo time msec], flip angle of 150°) with a total of six acquisitions – one before and five after intravenous injection of MR contrast (0.5 mmol/ml, Gadodiamide, Omniscan, GE Healthcare) at 3ml. Each volume consisted of 144 slices (1mm thickness) with a matrix size of 448 x 300 and field of view of 250-350mm depending on breast size. The resulting voxel size was 0.7 x 0.7 x 1mm and temporal resolution was 90sec. Because data collection from the two imaging modalities does not interfere, optical data was typically acquired twice per subject as time permitted. The first data set was used for analysis.

3. Results

3.1 Sensitivity analysis

The effects of spatial sensitivity were analyzed first by calculating the relative sensitivity to each lesion for each exam. The relative sensitivity of each lesion in malignant and benign groups is summarized in Fig. 3. The group of patients with a cancer diagnosis (n = 28) yielded a mean tumor sensitivity of 3.5% whereas the group with benign diagnoses (n = 16) showed a slightly lower mean of 3.3%, although no statistical difference ($p = 0.86$) was found between two groups, indicating that the measurements were not significantly different in terms of their sensitivity to malignant versus benign lesions.

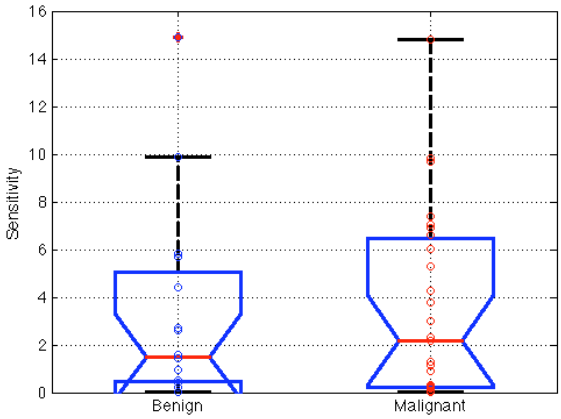

Fig. 3. Relative tumor sensitivity for malignant (n = 28) and benign (n = 16) lesions according to surgical pathology, showing no statistical difference between them in this estimate of sensitivity in the clinical data. Box ends show 25th and 75th percentile and two data sets with non-overlapping intervals are significantly different.

Measurement sensitivity had a large effect on recovery of tumor chromophore concentrations in the malignant versus benign cases. The subject exams were sorted from the most to least sensitive, and reconstructed chromophore concentrations were compared to surgical pathology in lesions with descending sensitivity. *P*-values for differentiating malignant from benign lesions based on total hemoglobin concentration (HbT), scattering amplitude (SA) and Tissue Optical Index (TOI) [21] as a function of relative tumor sensitivity to the measurement data are presented in Fig. 4. *P*-values from TOI were significant ($p<0.05$) when relative tumor sensitivity was above 1.2%, and TOI was maximally significant above a relative tumor sensitivity of 2.5% ($p = 0.00019$). Total hemoglobin (HbT) was also a significant indicator when sensitivities above 1.2% were included. These benign and

#214026 - $15.00 USD Received 16 Jun 2014; revised 8 Aug 2014; accepted 8 Aug 2014; published 22 Aug 2014

malignant groups were maximally different when imaging exams with sensitivity above 2.5% were included ($p = 0.0037$). Scatter amplitude was nearly significant when the tumor sensitivity was above 1.2% ($p = 0.09$).

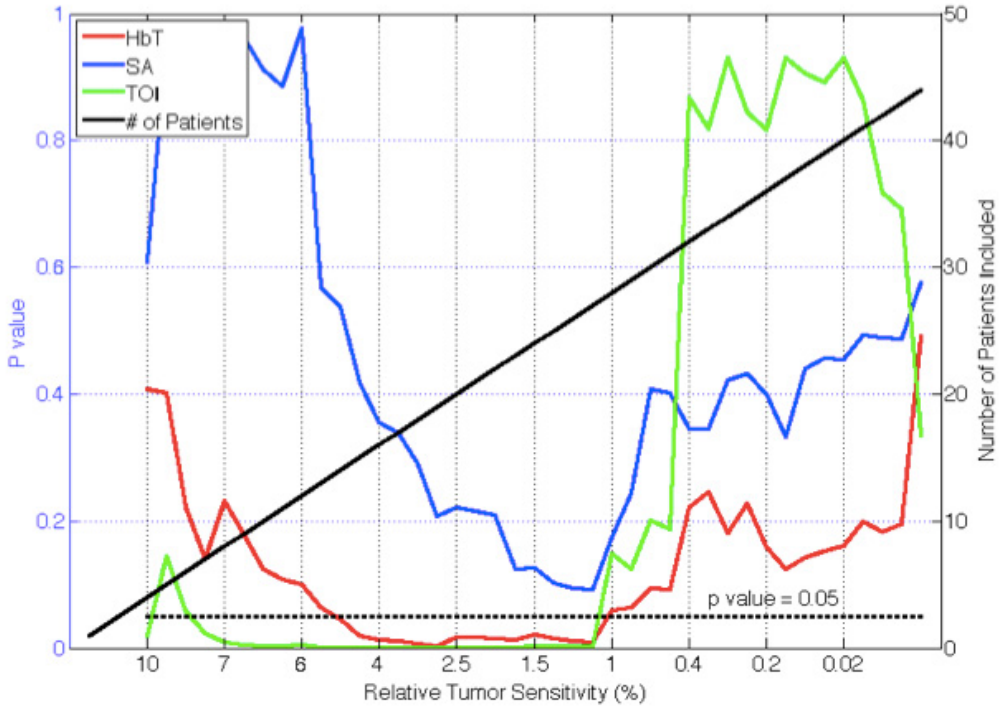

Fig. 4. P-values for differentiating malignant from benign lesions in recovered chromophores (HbT, SA, TOI) are plotted as a function of relative lesion sensitivity. Number of patients included in the analysis (right axes) for a given relative lesion sensitivity is indicated by the solid (black) line. As the number of patients included in the analysis increases, the associated p-values decrease until approximately 1% sensitivity.

3.2 Reconstruction type

After sorting the patient exam data by lesion sensitivity, p-values for separating malignant from benign abnormalities were compared for constrained and unconstrained spectral reconstructions in Fig. 5. In the constrained spectral reconstructions, the p values from TOI and HbT exhibited significance ($p<0.05$) when lesion sensitivity was greater than 1.2% whereas only HbT and SA were significant predictors of malignancy in the unconstrained spectral reconstructions. HbT achieved statistical significance for lesion sensitivity above 0.5% while SA was significant through nearly the entire sensitivity range. HbT was maximally significant above 1% sensitivity ($p = 0.015$) whereas SA was maximally significant above 1.3% sensitivity ($p = 0.012$).

#214026 - $15.00 USD Received 16 Jun 2014; revised 8 Aug 2014; accepted 8 Aug 2014; published 22 Aug 2014

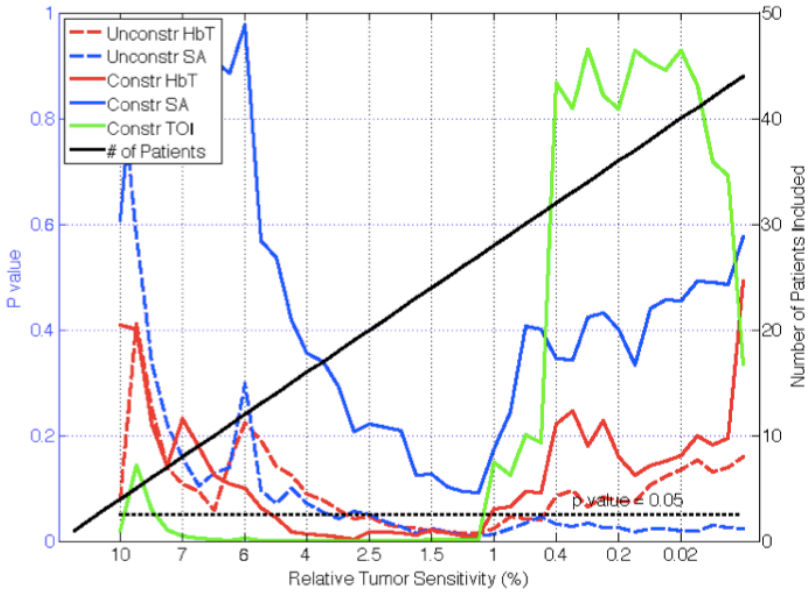

Fig. 5. P-values for differentiating malignant from benign lesions in recovered chromophores are plotted as a function of relative lesion sensitivity (left axes) for constrained and unconstrained spectral reconstructions. Number of patients included in the analysis (right axes) for a given relative lesion sensitivity is indicated by the solid (black) line. Unconstrained reconstructions separate malignant from benign lesions in more patients in HbT and SA.

3.3 Regularization parameters

To investigate the effects of regularization, constrained spectral reconstructions were performed on all patients with three different starting regularization parameters (1, 0.1, and 0.01) in Fig. 6. These values were selected after varying the initial regularization from 0.001 to 1.0 in two representative cases – one malignant and one benign – and concluding that regularizations much above unity smoothed the lesion-to-background contrast excessively (i.e. nearly to unity) and below 0.01 led to unstable results.

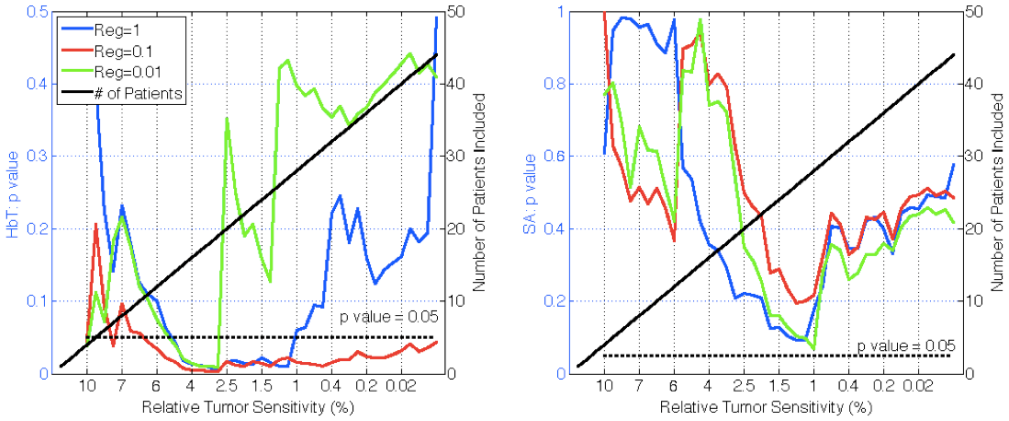

Fig. 6. The p-values of malignant versus benign groups in recovered chromophores HbT and SA are plotted versus relative tumor sensitivity (left axes) for three different regularizations in constrained spectral reconstructions. Also shown is the number of patients included (right axes). A regularization of 0.1 is the most effective for HbT, adequately smoothing noise but allowing image contrast to persist. SA requires a lower regularization of 0.01 to be most effective but does not reach statistical significance.

#214026 - $15.00 USD Received 16 Jun 2014; revised 8 Aug 2014; accepted 8 Aug 2014; published 22 Aug 2014

These data show that the HbT signal was diagnostic at a statistically significant level ($p<0.05$) for nearly the full data set when the regularization was equal to 0.1. At $\lambda = 1$, significance was achieved in lesions with sensitivity above 1.2%, and at $\lambda = 0.01$ significance was achieved in lesions with sensitivity above 3%. Regularization of $\lambda = 0.1$ was maximally significant above 3% tumor sensitivity ($p = 0.03$), but reconstructed values were not entirely reasonable physiologically. SA was not as good an indicator, with no λ value yielding statistical significance in any patient group, although $\lambda = 0.01$ was nearly significant ($p = 0.068$) for lesion sensitivities above 1%. As evidenced by the differences in these results, the value of λ has a large effect on the entire data set as well as on individual cases.

4. Discussion

4.1 Sensitivity analysis

Results in the literature indicate that NIRS imaging performance degrades as a function of distance from the imaging plane [34,35]. Accordingly, a measure to quantify the sensitivity of the measurements to the region of interest (ROI) should exist for each subject that could be applied prior to interpreting the data. Contrast-detail studies in NIRS imaging have also demonstrated that region size plays an important role in determining the minimum recoverable contrast [36,37]. The method described here to quantify tumor sensitivity to the measurement data is easy to apply and provides a quantitative metric for assessing the likelihood that the NIRS exam is adequately interrogating the lesion of interest.

Although the method does not currently separate the influence of lesion size from lesion location, many of the ROIs in the exam series evaluated suggest that lesion location is the more important consideration. Further, changes in tumor radius create cubic changes in tumor volume whereas the Jacobian contributions change by several orders of magnitude over a span of centimeters. Nonetheless, understanding the effects of lesion size versus lesion location warrants additional investigation.

Encoding sensitivity assessment into the exam data prior to image reconstruction provides a vehicle for determining which measurements have the most influence on the ROI within the reconstruction. This information is important because the measurement data can be noisy by being outside the linear range of the detector, or containing artifacts from poor fiber coupling, or suffer from low signal strength due to high absorption in the tissue and the sensitivity assessment can help distinguish noisy data from data through highly absorbing regions.

In this study, the benign (n = 16) and malignant (n = 28) lesion groups had mean tumor sensitivities of 3.3% and 3.5%, respectively. However, the exam data was not significantly different in sensitivity between the two lesion groups indicating that the imaging technique was equally sensitive to the two diagnostic categories. Ensuring complete breast coverage or the ability to accurately target the lesion with prior knowledge of its location would improve the sensitivity of the optical measurements to the ROI. Many of the lesions evaluated here were targeted based on palpation but without the assistance of prior imaging.

After sorting the exams by their relative lesion sensitivity, analysis of the most sensitive exams did not result in statistical differences between the malignant and benign groups, likely due to a small sample size ($n<6$). As the sample size increased, the confidence that the two groups come from different distributions increased. When tumor sensitivities greater than 2.5% were considered, the malignant and benign groups could be distinguished with statistical significance in both HbT and TOI ($p = 0.0037$ and $p = 0.00019$, respectively). Both of these parameters remained significant at the $p = 0.05$ level until the relative lesion sensitivity fell to 1%. When exams with less than 1% sensitivity to the region of suspicion were included, the malignant and benign distributions became inseparable, most likely because the measurements were no longer adequately probing the ROI, in which case its influence on the measured data is lost within the normal variation of the optical measurements, and contrast recovery is no longer possible.

These results suggest that diagnostically accurate data arises from cases where the lesion is adequately sampled, ideally with greater than 2.5% sensitivity, but with a minimum

#214026 - $15.00 USD Received 16 Jun 2014; revised 8 Aug 2014; accepted 8 Aug 2014; published 22 Aug 2014

sensitivity of at least 1%. Lesion sensitivity can be improved by targeting the abnormality based on prior knowledge of its position or with more complete coverage of the breast volume during NIRS data acquisition. Our single plane fiber interface allowed for targeting of lesions, but accurate placement was difficult in practice. Future designs of the MRI/optical breast coil should emphasize more complete coverage of all breast sizes. Even with incomplete coverage, the sensitivity parameter investigated here can be calculated prospectively on data where the tissue-fiber geometry and the suspected lesion geometry are known from the MRI scans.

4.2 Reconstruction types

While first introduced by Li et al, Brooksby et al, and Guven et al, prior information is known to improve NIRS image quantification in simulation, phantoms, and patient exams [38–41]. Studies have considered both spectral and spatial priors, as well as more sophisticated information such as water maps from simultaneous MR imaging [42–44]. While the benefits of incorporating prior information are well-established for NIRS imaging, when prior information is most effectively incorporated remains less clear [21,45,46]. Here, data was reconstructed using spatial and spectral priors but the spectral priors were applied at two different times.

Specifically, the unconstrained spectral reconstruction method was able to statistically differentiate distributions of the benign and malignant tumor to adipose ratios in HbT and SA. Both chromophores were statistically significant when lesion sensitivity exceeded 0.5%. They were maximally significant when exams with lesion sensitivity above 1% were included ($p = 0.015$ for HbT, $p = 0.012$ for SA). Although StO_2, H_2O, lipid, and TOI concentrations were also obtained, they were not diagnostically significant indicators, likely because these chromophores were not constrained during the reconstruction process. Only three wavelengths were sensitive to important spectral features of water and lipids in the current MRI/optical system (903, 912, and 948nm), thus, not enough spectral sensitivity was available to calculate these chromophores accurately after reconstruction when tumor sensitivity was low. Similarly to previous results, HbT and SA were good indicators of breast malignancy, and the unconstrained reconstruction method would be expected to produce promising results in a larger patient study [31,47].

When the constrained spectral reconstruction method was applied, HbT and TOI were the most significant indicators of tissue malignancy. They were maximally differentiating when tumor sensitivity was above 2.5% ($p = 0.0037$ for HbT, $p = 0.00019$ for TOI). Scatter amplitude was not significantly diagnostic (minimum $p = 0.09$) in this case. The constrained reconstruction required higher lesion sensitivity to achieve diagnostic significance in HbT and TOI relative to its unconstrained counterpart (2.5% vs. 1%). Although SA and HbT did not perform as well in the constrained case based on lesion sensitivity, they separated the malignant and benign group means with greater confidence when lesion sensitivity was greater than 1%. TOI calculated from the constrained reconstructions was the best overall predictor ($p = 0.00019$) and will continue to be an important breast tumor indicator along with HbT [48]. Though both algorithms are able to different malignant lesions from benign it is not possible to know the correct optical properties of each breast. Therefore, it can't be said which algorithm is more accurate in an absolute sense and we leave that to a future investigation.

4.3 Regularization parameter

The starting value of λ produces the maximum amount of smoothing and noise suppression since lambda is scaled with respect to model-data mismatch. As the reconstruction is optimized, lambda decreases. Therefore, very noisy data requires a higher starting value to adequately suppress noise [27,36]. If the starting value is too high, the regularization can also suppress the contrast in the data. Specifically, when the regularization was set very high, above 1, the image contrast was significantly dampened and nearly homogeneous images were recovered. When the regularization was too low, under 0.01, the reconstructions became

#214026 - $15.00 USD Received 16 Jun 2014; revised 8 Aug 2014; accepted 8 Aug 2014; published 22 Aug 2014

unstable as the noise suppression was not sufficient and the image failed to converge to a physiologically valid solution. Furthermore, small changes in λ caused large changes in chromophore concentrations. A region of stability existed in the middle of the range, from 0.01 to 1, where images converged to physiologically expected values and small changes in regularization produced small, predictable changes in the resulting images.

While minimizing λ within the region of image stability for individual patient reconstructions is ideal, the same λ value was used in all reconstructions. The amount of regularization required varies with breast density, optical fiber placement, noise within the measurements, and other factors [24]. Therefore, regularization must be chosen to suppress noise adequately while still allowing image contrast to be recovered in most patients. For HbT as an example chromophore, $\lambda = 0.1$ was able to best suppress noise while allowing image contrast. This value achieved statistical significance in HbT for all levels of lesion sensitivity; however, we found it was not optimal for the other chromophores that might require more noise suppression such as H_2O, lipids, and scatter. These latter chromophores favored a higher regularization, and $\lambda = 1$ was the best match for all chromophores. While this value yielded some unwanted smoothing in HbT, results were still diagnostically significant for lesion sensitivity above 1%, and favorable in the other chromophores, which benefited from the increased noise suppression.

5. Conclusions

In this study, data from breast MRI-guided near infrared spectroscopy were analyzed from a group of 44 breast exams delivered to patients already planned for surgery (16 benign, 28 malignant diagnoses). Results show that optical measurement sensitivity, reconstruction constraints, and regularization parameter were important factors in determining the diagnostic significance of the MRI/optical exam. MRI/optical data was able to differentiate malignant from benign lesions in both HbT ($p = 0.0037$) and TOI ($p = 0.00019$), but required that relative spatial sensitivity in the measurements be above a 1% threshold. Lesion sensitivity was the most critical factor and no diagnostic significance was found when exam data with very low region of interest sensitivity were included in the analysis. Spectral constraints were required to obtain clinically diagnostic information from optical measurements of H_2O, lipids, and TOI. The ideal regularization parameter varied case by case, and must be carefully selected to reduce image noise adequately, while still allowing sufficient image contrast.

Acknowledgments

This work was funded by NIH grant R01 CA069544 and National Natural Science Foundation of China grant 81101091.

#214026 - $15.00 USD Received 16 Jun 2014; revised 8 Aug 2014; accepted 8 Aug 2014; published 22 Aug 2014